Reverse annealing of boron doped polycrystalline silicon

Jung-Yoon Lim[1], Won-Eui Hong[1], Deok Hoi Kim[2], Tstomu Uemoto[2], Chi Woo Kim[2] and Jae-Sang Ro[1]
[1]Dept. of Materials Science and Engineering, Hongik Univ. Seoul, 121-791, Korea
Phone: 82-2-320-1698, E-mail: jsang@wow.hongik.ac.kr
[2]LTPS Team, AMLCD Business, Samsung Electronics, Yongin-City, Gyeonggi-Do, 449-711, Korea

Keywords : reverse annealing, ion implantation, activation

Abstract

Through-doping conditions with higher energies and doses were intentionally chosen to understand reverse annealing behavior. We observed that the implantation condition plays a critical role on dopant activation. We found a certain implantation condition with which the sheet resistance is not changed at all upon activation annealing.

1. Introduction

Non-mass analyzed ion shower doping (ISD) technique with a bucket-type ion source or mass-analyzed ion implantation with a ribbon beam-type has been used for source/drain doping, for LDD (lightly-doped-drain) formation, and for channel doping in fabrication of low-temperature poly-Si thin-film transistors (LTPS-TFT's) [1,2,3]. We reported an abnormal activation behavior in boron doped poly-Si at IDW '06 where reverse annealing, the loss of electrically active boron concentration, was found in the temperature ranges between 400℃ and 650℃ using isochronal furnace annealing [4]. We also reported reverse annealing behavior of sequential lateral solidification (SLS) poly-Si using isothermal rapid thermal annealing (RTA) [5]. We report here the importance of implantation conditions on the dopant activation.

2. Experimental

For the sample preparation SiO2 insulation layer with a thickness of 300 nm was formed on a glass substrate of 370 mm x 470 mm x 0.7 mm (width x length x thickness) by means of plasma enhanced chemical vapor deposition (PECVD). An a-Si thin film with a thickness of 50 nm was formed successively upon the insulation layer using PECVD. The substrates used were poly-Si produced by two-shot SLS followed by deposition of 75 nm-thick SiO_2 layer. The glass substrate was broken into pieces of 20 mm x 20 mm, thereby preparing a test piece. Boron was implanted by mass-separated ion implanter with acceleration energies from 20 to 35 keV. RTA annealing was conducted in the temperature ranges from 550℃ to 650℃ for dopant activation. The sheet resistance was determined using a 4-point-probe. Activation efficiency and mobility of charge carriers were determined by Hall measurement using a van der Paw method.

3. Results and discussion

Table 1 shows implantation conditions for the 5 samples implanted with acceleration energies from 20 to 35 keV and at doses from $1x10^{15}/cm^2$ to $4x10^{15}cm^2$. We conducted TRIM-code simulation to calculate the concentration profiles of implanted boron atoms and induced defects. Simulated concentration profiles were in good agreement with the results obtained by secondary ion mass spectroscopy (SIMS). Actual doses were also verified using SIMS. Figure 1 shows them as a function of acceleration energies. As indicated in Fig. 1 concentration of boron and defect decreases sharply in 50 nm thick poly-Si implanted especially with acceleration energy of 20 keV. Table 1 illustrates implantation conditions for the 5 samples and denotes the effective dose and the effective defect density accumulated in Si-layer according to TRM-code simulation. As indicated in the table the sample #Pe has the largest effective defect density (~ $2x10^{17}/cm^2$) while the samples #Pb and #Pd have the second largest value (~ $1x10^{17}/cm^2$) and #Pa and #Pc have the smallest one (~ $5x10^{16}/cm^2$).

TABLE 1. Implantation conditions for the 5 samples used in this work and the corresponding effective dose and the effective density accumulated in 50 nm –thick poly-Si according to TRIM-code simulations.

	Pa	Pb	Pc	Pd	Pe
Acceleration voltage (keV)	20	20	30	30	35
Dose (#/cm^2)	2×10^{15}	4×10^{15}	1×10^{15}	2×10^{15}	4×10^{15}
Effective Dose (#/cm^2)	3.91×10^{14}	7.82×10^{14}	2.42×10^{14}	4.84×10^{14}	1.06×10^{15}
Effective Defect Density (#/cm^2)	5.15×10^{16}	1.03×10^{17}	5.2×10^{16}	1.04×10^{17}	2.02×10^{17}

Figure 2 shows the sheet resistance as a function of annealing time and temperature for each sample. As indicated in Fig. 2 the sheet resistance is not sensitive to annealing time. As indicated in Fig. 2 we found that the values of sheet resistance could be divided into 3 groups. Each group represents the sample implanted with the same energy. It is interesting to note that the sheet resistance of the sample, Pe, is not sensitive to annealing temperature (550~650°C) and annealing time (15-180s) at all.

Figure 3 shows activation fraction, sheet carrier concentration divided by actual dose, as a function of annealing time for the 5 samples annealed at 550℃, 600℃ and 650℃, respectively. Similar to the results of the sheet resistance shown in Fig. 2 the activation fraction may be divided into 3 groups which depend on implantation energies. The samples implanted with higher energies were observed to show higher activation fraction. The value of activation fraction for the samples, $\#P_a$ and $\#P_b$, implanted with lower energy of 20 keV annealed at 550°C is around 0.2. As we annealed the samples at 650°C it decreases to the value less than 0.15. The activation fraction also decreases slightly with annealing time at each annealing temperature. These samples exhibit distinctive behavior of reverse annealing. Meanwhile the activation fraction of the sample $\#P_e$, implanted with the highest energy and dose, does not change at all as the annealing temperature increases from 550°C to 650°C. All samples except the sample $\#P_e$ show reverse annealing behavior as the annealing temperature increases from 550°C to 650°C. The magnitude of activation fraction of the samples annealed at 650°C, the highest RTA temperature investigated in this work, has a higher value as the implantation energy increases. Under the same implantation energy it has a higher value as the dose increases. At 650°C it has the following order; $\#P_e$ (35keV, $4x10^{15}/cm^2$) > $\#P_d$ (30keV, $2x10^{15}/cm^2$) > $\#P_c$ (30keV, $1x10^{15}/cm^2$) > $\#P_b$ (20keV, $4x10^{15}/cm^2$) > $\#P_a$ (20keV, $2x10^{15}/cm^2$).

We reported reverse annealing of poly-Si [5,6]. In the previous study we found that the reverse annealing already begins at annealing temperatures less than 400°C when using furnace annealing. As known well reverse annealing is related to silicon self-interstitials released from the ion induced damage-region. Thus damage recovery would be required for reverse annealing. It seems that damage recovery of the samples having higher defect density in 50 nm-thick poly-Si sandwiched between oxide layers would require higher thermal budget. In table 1 we showed the effective defect density accumulated in 50 nm-thick poly-Si calculated by integrating defect concentration profile between 75 nm to 125 nm. If we only consider this argument efficiency of the activation fraction at 650°C would be as follows according to TRIM-code simulation as indicated in Table 1; $\#P_e$ (35keV, $4x10^{15}/cm^2$) > $\#P_d$ (30keV, $2x10^{15}/cm^2$) > $\#P_c$ (30keV, $1x10^{15}/cm^2$) = $\#P_b$ (20keV, $4x10^{15}/cm^2$) > $\#P_a$ (20keV, $2x10^{15}/cm^2$). This order, however, does not match with our experimental results as shown in Fig. 3(c). Integrated defect density alone, therefore, may not explain our findings. What is more important, we propose, is not integrated defect density but defect concentration profile itself. As we already pointed out defect concentration decreases rapidly in 50 nm-thick poly-Si for the samples implanted with acceleration energy of 20 keV as can be seen in Fig. 1(a). Although the magnitude of integrated defect density of the sample $\#P_b$ (20keV, $4x10^{15}/cm^2$) is very similar to that of the sample $\#P_d$ (30keV, $2x10^{15}/cm^2$) activation fraction of the sample $\#P_d$ is higher than that of $\#P_b$. Damage recovery may occur in the bottom part of poly-Si where defect concentration decreases significantly for the samples implanted with lower energies. Then reverse annealing could be observed as the annealing temperature increases. Figure 4 shows Hall mobility as a function of annealing time for the 5 samples annealed at (a) 550℃, (b) 600℃, and (c) 650℃, respectively. Changes of Hall mobility are not so sensitive for the samples implanted with severe conditions of higher energies and doses. Hall mobility does not almost change for the sample $\#P_e$ while it increases significantly as the annealing temperature and time increase for the sample $\#P_a$. The present experimental results reveals that a certain implantation condition does exist, which does not induce reverse

annealing.

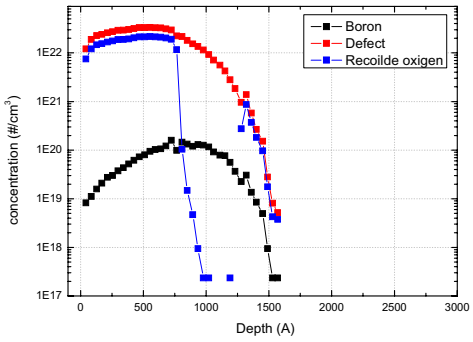

(a) 20keV

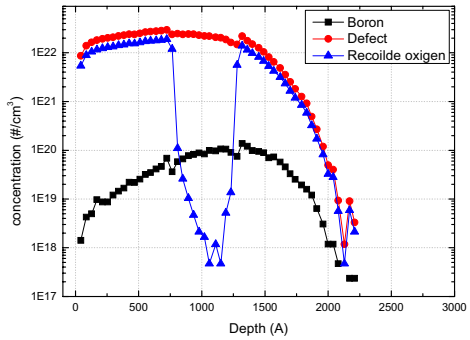

(b) 30keV

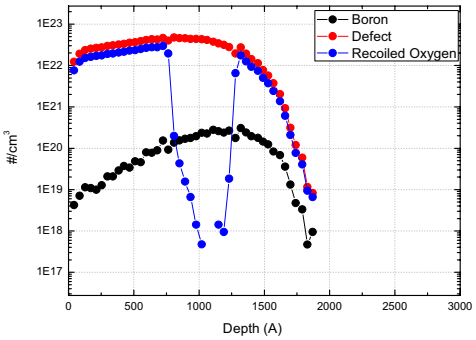

(c) 35keV

Fig. 1. Simulated concentration profiles of implanted boron and induced defect calculated using a TRIM-code. Notice that the both of concentration drops rapidly in 50 nm thick poly-Si implanted especially with acceleration energy of 20 keV.

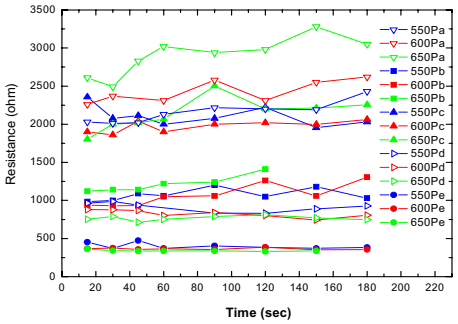

Fig. 2. Sheet resistance vs annealing time and temperature for the 5 samples

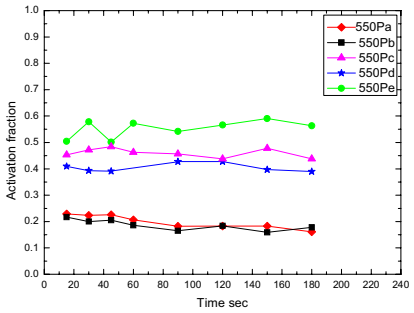

(a)

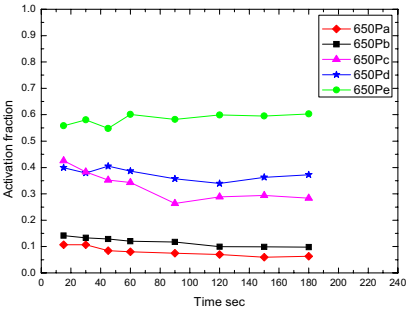

(b)

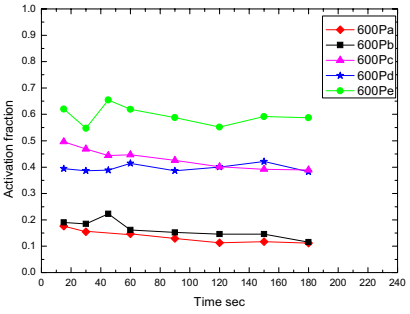

(c)

Fig. 3. Activation fraction vs annealing time with various implantation conditions annealed at (a) 550℃ (b) 600℃ and (c) 650℃, respectively.

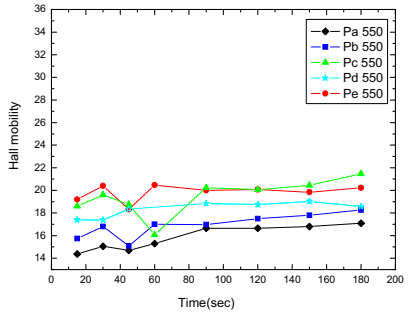

(a)

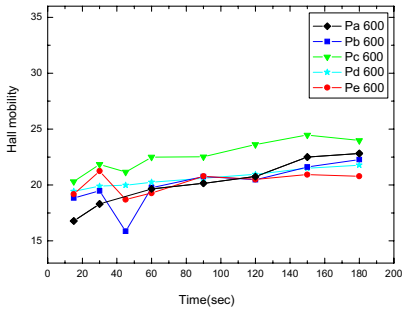

(b)

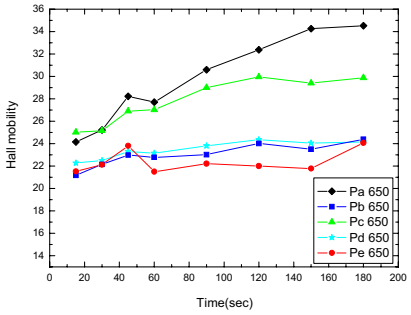

(c)

Fig. 4. Hall mobility vs annealing time with various implantation conditions annealed at (a) 550℃ (b) 600℃ and (c) 650℃, respectively.

4. Summary

The reverse annealing was previously observed in the boron implanted SLS poly-Si with lower energies and doses. In this work we found that we could control reverse annealing behavior by varying the implantation conditions. We believe that the defect concentration profile may be important to annealing behavior of poly-Si rather than integrated defect density accumulated in the silicon layer. Based on the present findings it is worthwhile to note that wise choice of implantation conditions may play a critical role in preventing the non-uniformity problem of sheet resistance over the large area glass substrate upon RTA dopant annealing in the mass production line.

5. Acknowledgements

This work was supported by Samsung Electronics Company.

6. References

1. A. Yoshida, K. Setsune, and T. Hirao, *Appl. Phys. Lett*, **51**, 252 (1987)
2. G. Kawachi, T. Aoyama, K. Miyato, Y. Ohno, A. Mimura, N. Komishi, and Y. Mochizuki, *J. Electrochem. Soc*, **137**, 3522 (1990)
3. Yasuyoshi Mishima and Michiko Takei, *J. Appl. Phys*, **75**, 4933 (1994)
4. 4. B.-J. Jin, S.-J. Oh, D. H. Kim, T. Uemoto, C W Kim and J.-S. Ro, IDW ’06 Technical Digest p 769 (2006)
5. B-J Jin, W-E Hong, J-Y Lim, D-H Kim, T Uemoto, C-W Kim and J-S Ro, IMID ’07 Technical Digest p 769 (2007)
6. B-J Jin, W-E Hong, D-H Kim, T Uemoto, C Woo Kim, J-S Ro, *Thin Solid Films,* **516** p 6321–6324 (2008)